Noor, Imtisal e.; Coenen, Jan; Martin, Andrew; Dahl, Olli

Performance assessment of chemical mechanical planarization wastewater treatment in nano-electronics industries using membrane distillation

Published in:
Separation and Purification Technology

DOI:
10.1016/j.seppur.2019.116201

Published: 18/03/2020

Document Version
Publisher's PDF, also known as Version of record

Separation and Purification Technology 235 (2020) 116201

Contents lists available at ScienceDirect

Separation and Purification Technology

journal homepage: www.elsevier.com/locate/seppur

Performance assessment of chemical mechanical planarization wastewater treatment in nano-electronics industries using membrane distillation

Imtisal-e- Noor[a,b,*], Jan Coenen[c], Andrew Martin[a], Olli Dahl[b]

[a] Department of Energy Technology, KTH Royal Institute of Technology, Stockholm, Sweden
[b] Department of Bioproducts and Biosystems, Aalto University, Espoo, Finland
[c] Interuniversity Microelectronics Center (imec), Leuven, Belgium

ARTICLE INFO

Keywords:
Chemical mechanical planarization
Separation efficiency
Membrane distillation
Nano-electronics
Energy analysis

ABSTRACT

Wastewater from chemical mechanical planarization (CMP) processes in nano-electronics industries must be treated properly in order to fulfil local and international environmental regulations. This study is focused on a performance assessment of membrane distillation (MD) technology for CMP wastewater treatment. A new prototype of air gap membrane distillation (AGMD) module was utilized, with feed water consisting of CMP wastewater collected from imec, Belgium. The module was tested at different operating conditions (temperatures, flow rates and filtration time) and responses in terms of separation efficiency, permeate water quality, transmembrane flux, specific heat demand and exergy efficiency were determined. High quality permeate was produced in all trials, i.e. conductivity ~2.11 μS/cm, pH ~5.4, TOC ~1.13 ppm, IC ~0.24 ppm, TDS ~1.18 ppm and COD ~ 1.9 ppm; for most of the contaminants the separation efficiency was > 99%. These findings clearly show that the resulting MD permeate does not exceed environmental regulations for release to recipient, and the permeate can even be considered for reuse. Moreover, the determined specific heat demand at different operating conditions was varying between 1390 and 2170 kWh/m^3 whereas; the achievable exergy efficiency was ~19%.

1. Introduction

In the 1980s chemical mechanical planarization (CMP) was introduced at IBM for integrated circuit (IC) fabrication, later emerging as a crucial polishing technique in nano-electronics industries [1]. In CMP processes abrasive materials (amorphous silica, alumina and ceria) [2] are used in combination with ultrapure water and a range of chemical additives: complexing agents (amino acids and carboxylic acids) [3]; oxidizers (hydrogen peroxide, ferric nitrate and potassium permanganate) [4]; corrosion inhibitors (benzotriazole and aminotriazol) [5]; pH adjustors (hydrochloric acid, potassium hydroxide, nitric acid, ammonium hydroxide and buffers) [4]; surface active agents (polyacrylic acid, polyethylene glycol and cetyltrimethylammonium bromide) [6,7]; high molecular weight polymers (polyethylene oxide) [4]; and biocides [6]. According to Babu [8] around 0.2–0.8 L of CMP slurry is employed per produced wafer, leading to a wastewater stream of about 7–10 L per wafer. The produced wastewater contains approximately 3–12% solids by weight and pH levels range from 6.8 to 10. Moreover, the total organic carbon (TOC) levels are distributed between 2 and 15 mg/L. Total concentrations of used silica and alumina in wastewater as reported in the literature [9–11] are 98–4000 mg/L (0.05 to 0.2% solids) and 0.01–11.8 mg/L respectively.

With an ever-growing application of CMP technology in nano-electronics industries, the amount of CMP wastewater has increased exponentially and is thus attaining considerable attention. Typically, the fresh water demand of a nano-electronics manufacturing plant ('fab') is approximately 1000 m^3/day where 30–40% of total is accounted by CMP processes [12,13]. To observe EU Directive 91/271/EEC concerning urban wastewater treatment [14], CMP-derived wastewater needs to be treated by removing nano-sized amorphous silica, alumina, ceria, and other chemical contaminants prior to discharge. Traditional chemical coagulation/flocculation treatment processes involve high dosage of chemicals (polyvalent electrolytes such as calcium, aluminum, and iron salts) to help solids content agglomerate and settle down for removal through subsequent filtration [15,16]. These processes lead to high operational costs due to high chemical demand and sludge disposal costs. Moreover, such operations are unable to ensure a high separation efficiency for the typical contaminant concentrations.

A number of alternate CMP wastewater treatment methods have been presented and analyzed by several researchers and include

* Corresponding author.
E-mail address: ieno@kth.se (I.-e.-. Noor).

https://doi.org/10.1016/j.seppur.2019.116201
Received 20 May 2019; Received in revised form 27 September 2019; Accepted 9 October 2019
Available online 11 October 2019

processes involving electro-chemical separation, membrane separation, and other methods. Within the first category, Belongia et al. [17] studied electro-decantation and electro-coagulation for removing and reusing alumina and silica from CMP waste. The findings illustrated that the coupled method has the potential to agglomerate and recover alumina and silica. Lia et al. [12,18] used an aluminium/iron electrode pair and observed 96.5% turbidity removal and 75–85% chemical oxygen demand (COD) reduction with an effluent COD of below 100 mg/l. Yang et al. [19] investigated electro-microfiltration considering pulsed mode, no electric field mode and continuous mode operations for treatment of CMP wastewater. The outcomes showed that the continuous mode operation displayed the optimized results i.e., high quality filtrate having turbidity as low as 0.39 NTU. Further, coupled electro-microfiltration and electro-dialysis has also been examined by these researchers [20]. Coupling the two methods yielded a permeate/filtrate suitable for high level recycling; obtained permeate exhibited turbidity < 1 NTU, TOC < 3 mg/l, and total dissolved solids (TDS) < 50 mg/l. Hu et al. [21] performed experiments with aluminium electrodes for electro-coagulation and flotation process. A turbidity reduction of 90% was observed while adding cationic surfactant cetyltrimethylammonium bromide (CTAB). Den et al. [22] presented the effect of hydraulic retention time and applied current density on turbidity reduction. Iron anodes and stainless steel cathodes were used in this study to reach removal efficiency of 95%. Liu et al. [23] studied electro-coagulation using iron electrodes for treating the CMP wastewater. The outcomes showed that the particles removal efficiency was ~ 99% at a current density of 5.9 mA/cm^2. Wang et al. [24] revealed that iron/aluminium electrode pair is relativity an efficient choice as compared to other typical electrode pairs for electro-coagulation in terms of energy demand. Finally, Chou et al. [25] investigated thermodynamic aspects of the electro-coagulation for oxide CMP wastewater treatment and demonstrated that the system operation was endothermic and spontaneous between 288 and 318 K.

Membrane based processes have also been investigated for CMP wastewater treatment. Brown et al. [26], Lin et al. [27] and Juang et al. [28] showed the performance of ultrafiltration (UF) and reverse osmosis (RO) in this regard. Brown et al. [26] demonstrated that metal and mixed oxide CMP wastewater can be treated and reused using ultrafiltration (UF). Lin et al. [27] considered chemical coagulation and reverse osmosis (RO) for CMP wastewater treatment for reuse. High quality permeate has been recovered after removing 99% of alumina and silica, and lowering the CMP wastewater COD < 100 mg/l. Juang et al. [28] investigated an arrangement of integrated UF and RO for CMP wastewater treatment for reuse. The results showed permeate having turbidity ~0.01 NTU, conductivity ~6 μS/cm and TOC ~1.6 mg/L.

Other approaches for CMP wastewater treatment include use of magnetic seeds along with chemical coagulant to enhance aggregation and precipitation of alumina and silica. Wan et al. [29] indicated that turbidity of the CMP wastewater could be reduced from 1900-2500 NTU to 23 NTU with the action of 3.74 g L^{-1} magnetite ($FeO*Fe_2O_3$) seeds using applied magnetic field of 1000 G. The coupling has significantly reduced the production of waste sludge as well. Kim et al. [30] tested the combined effect of magnetic separation and chemical coagulation on purification of CMP wastewater. The researchers employed magnetite (1.5 g/L) and ferric chloride (0.2 g/L) which displayed relatively better performance, reaching 0.94 NTU.

These processes have shown promise in certain applications, however there are significant challenges that prevent their widespread adaptation. Electrode-aided processes (electro-filtration/dialysis/coagulation) have the problem of reduced treatment efficiency due to electrode blockage. These processes are also cost-inefficient due to high electrical energy demand. Furthermore, microfiltration and ultrafiltration have the issues related to organic and inorganic fouling/scaling resulting in membrane blockage. Reverse osmosis is a pressure-driven separation technique and has a relatively high electrical energy demand. Additionally, high-pressure differences across the membrane require high mechanical strength of the membrane and induces biofouling (that needs to be treated using harsh chemicals). Moreover, treatment of large volume of CMP wastewater using magnetic seeding aggregation becomes unnecessarily expensive due to high cost of needed magnetic seeds. Thus, these practices are unreliable, energy inefficient, involve chemical treatments and are expensive.

Considering these limitations, membrane processes are judged to hold the most promise assuming that the following aspects can be addressed satisfactorily: reasonable pretreatment requirements; low fouling propensity; low chemical and electricity demands; and cost efficiency. Therefore, this study introduces membrane distillation as a promising method to treat CMP wastewater especially for removal of silica, alumina and copper. Membrane distillation (MD) is a thermally driven separation process utilizing a microporous hydrophobic membrane that only allows volatiles (i.e., water vapors etc.) to permeate through the membrane. The main driving force is a vapor pressure gradient across the membrane, which is developed due to temperature differences involved in the process [31–33]. The term MD originates from conventional distillation process modified with membrane separation [34]. The involved phase separation in MD process is based on the vapor-liquid equilibrium where latent heat of evaporation drives the change in phase from liquid to vapor [35]. The water transport through the membrane can be summarized in three steps: (1) formation of a vapor gap at the hot feed solution–membrane interface; (2) transport of the vapor phase through the microporous system; (3) condensation of the vapor at the cold side of the membrane–permeate solution interface [36]. As compared to other membrane technologies, MD operates at mild temperatures and atmospheric pressure. Moreover, it is relatively insensitive to pH and concentration fluctuations [34].

Furthermore, previous record of MD's successful applications for recovery of heavy metals [37,38], dehydration of organic compounds [39–41], concentration of acids [42–44], separation of pharmaceutical residues at very low to moderate concentrations [45,46], and wastewater treatment and water recovery [47–52] provides a strong argument to consider MD as a potential technology that can be successfully employed for treating wastewater streams contaminated with heavy metals, organic compounds, acids and nano-scale oxides i.e., CMP wastewater. We believe that this is the first work that shows the potential of MD technology for treatment of CMP wastewater. The present study is dedicated to a performance analysis of membrane distillation for CMP wastewater treatment. In this regard, separation efficiency of major contaminants is considered as the key performance factor whereas, conductivity, pH, TOC, COD and TDS are also determined in order to satisfy the water quality standards for reuse of the treated water in industrial utilities processes. Moreover, energy and exergy analyses have also been performed for a complete technical evaluation.

2. Methodology

2.1. Experimental apparatus

For all the experiments, a prototype air gap membrane distillation (AGMD) module supplied by Xzero AB has been employed, as presented in Fig. 1 [53]. The design of the Xzero AGMD module is based on the HVR AGMD module [54] with certain modifications (essential for MD application in nano-electronics fabs). The comparison shows that both of the AGMD modules consist of single-cassette (placed between two condensation plates) configurations employing two microporous hydrophobic polytetrafluoroethylene (PTFE) membranes. However, the way used for attaching the membranes to the polyethylene (PE) frame was thermal welding in case of HVR AGMD module and beam clamping in case of Xzero AGMD module. (The latter was used in order to avoid leakages and to cope with higher pressures on the membrane.) Flow spreaders were added to the cassette for improved heat and mass transfer. The air gap between the membrane and condensation plates

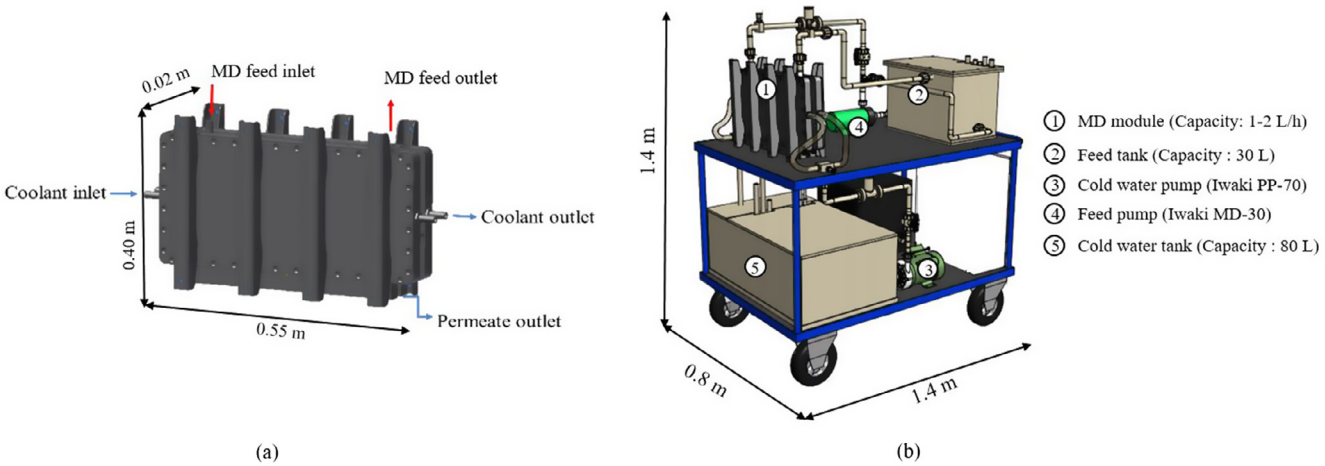

Fig. 1. (a) Membrane distillation module and (b) Xzero air gap membrane distillation bench scale unit [53].

was also reduced. Furthermore, in order to solve corrosion issues and for providing an inert environment, the condensation plates were covered with polyvinylidene fluoride (PVDF) on the permeate side in order to ensure high permeate quality.

The CMP wastewater (feed) is heated with a Teflon-coated immersion heater (capacity 2 kW) mounted in a 30 L PVDF feed storage tank. The heated water is then circulated towards AGMD module using an Iwaki MD-30 PVDF pump (magnetic coupled shaft) and controlled by an FIP FlowX3 paddlewheel flow sensor. The hot water is fed into the top of the MD module and the exiting (concentrated) feed recirculates back to the storage tank. Fresh water is cooled using a R1134a chiller (capacity: 1.8 kW) integrated with a 80 L PP cold-water tank. Using an Iwaki PP-70 pump, the cold water is circulated through the cooling plates. The flow rate of the cold-water has been controlled and measured with similar type of flowmeter as mentioned earlier. Permeate is collected at the base of the MD module and is measured with a graduated cylinder and stopwatch. The temperatures of hot and cold streams are measured with temperature sensors (pT100). All sensors and alarms are controlled by a Crouzet logic unit. A handheld conductivity meter and temperature sensor are used for checking the permeate conditions. In this unit, Donaldson® PTFE membrane is used considering its attractive cost–performance comparison. The characteristics of the used membrane are mentioned in Table 1 and the process flow diagram of the Xzero membrane distillation purification system is shown in Fig. 2.

2.2. Experimental procedure

A total of 100 L of CMP wastewater was collected in five 20 L samples from imec, Belgium during a ten day period (some variation in composition was inevitable owing to the changes in upstream trials). Samples 1, 2 and 3 were used to determine the separation efficiency of contaminants using the aforementioned Xzero AGMD module. Considering that concentration does not affect the parametric study significantly, the other two samples were considered to determine permeate yield and energy requirement.

Table 1
Characteristics of the membrane used in Xzero air gap membrane distillation module.

Membrane area (m^2)	0.194
Pore size (μm)	0.2
Porosity (%)	80
Thickness (μm)	254
Liquid entry pressure (kPa)	345

2.2.1. Separation efficiency

For CMP wastewater treatment tests, sample 1 (S1) was tested as MD feed without considering any pretreatment however, samples 2 and 3 (S2 and S3, respectively) were neutralized with 10 mL of 40% H_2SO_4 per 20 L of CMP wastewater samples prior to introduction into the MD modules. The samples S1, S2 and S3 were used in Test 1, Test 2 and Test 3, respectively. The nominal operating conditions for CMP wastewater treatment tests were as follows: MD feed inlet flow rate 7.2 L/min; cold-water inlet flow rate 8.3 L/min; MD feed inlet temperatures 85 °C for S1, 80 °C for S2 and 75 °C for S3; cold-water inlet temperatures 35 °C for S1, 30 °C for S2 and S3; and elapsed time of 3 h. Fluid flow conditions within the module indicate an average main flow channel velocity within a range of 0.025–0.055 m/s, assuming a U-type flow pattern from inlet to outlet. This condition corresponds to a Reynolds number range of 800–2500.

After achieving steady state, feed, retentate and distillate samples were taken in every 30 min, and the subsequent physico-chemical analysis included determination of cations (sodium, potassium and ammonium) concentration, anions (fluoride, chloride, nitrate, sulfate and phosphate) concentration, metals (aluminum, calcium, potassium, chromium, manganese, iron, nickel, cobalt, copper, zinc, gallium, strontium, phosphorous, germanium, tungsten, titanium, silicon, tantalum and zirconium) concentration, conductivity, pH, TOC, COD, IC (inorganic carbon), and TDS. For determining the mentioned water quality parameters, several analytical methods have been used. The pH was measured with an Orion Star Series meter with Orion Ross half-cell electrode and Ross reference electrode. The conductivity was determined using LF3000 with Pt-Cell (K = 0.1). The TOC (as well as IC and TC (total carbon)) was measured with Sievers 900 TOC-analyzer and COD was determined with Hach reagents LCI500. The anions and cations were measured with ion chromatography after adequate dilution on ThermoFischer ICS-5000 Capillary System. Metals were analyzed on ICP-OES from PerkinElmer.

The concentration factor of the contaminants in the MD feed over the elapsed time was also determined for each of the experiments. Concentration factor (CF_i) of the contaminants was defined by retentate to feed concentration ratio of contaminants as illustrated in Eq. (1):

$$CF_i = \frac{C_{R,i}}{C_{f,i}} \quad (1)$$

where $C_{R,i}$ depicts the retentate concentration of contaminant i and $C_{f,i}$ represents the concentration of contaminant i in MD feed water (wastewater).

Moreover, feed volume reduction factor (VRF) was also calculated in order to determine the degree of concentration of the feed for the elapsed time using Eq. (2).

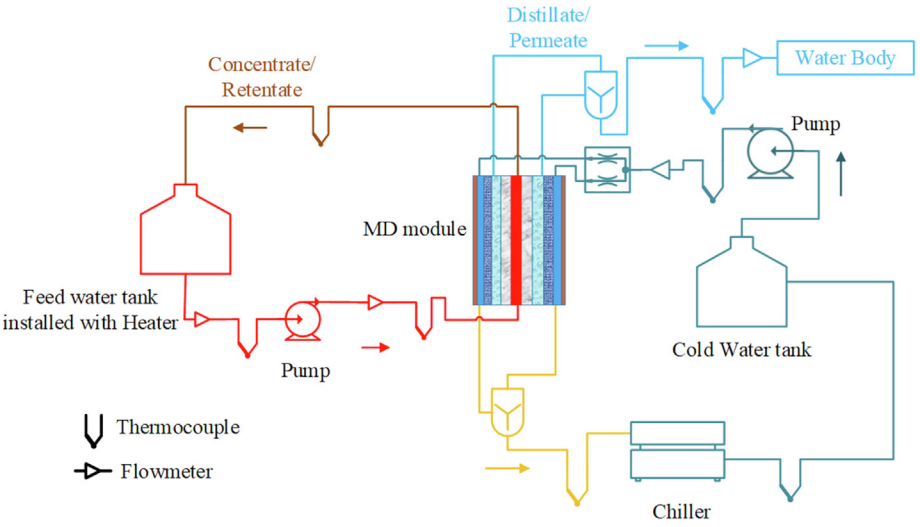

Fig. 2. Process flow diagram of Xzero air gap membrane distillation bench scale system.

$$VRF = \frac{V_d}{V_F} \quad (2)$$

where V_d defines the volume of permeate and V_F shows volume of initial MD feed.

2.2.2. Energy analysis

Typically, flow rates and temperatures have been considered as the critical variables that influence the transmembrane flux and thermal energy demand of AGMD system. The considered levels of these parameters for energy analysis were as follows: feed flow rates (3.5, 4.6, 5.3, 6.7 and 7.2 L/min), feed temperatures (67, 70, 75, 80 and 85 °C), cold-water flow rates (3.5, 6, 7.2 and 8.3 L/min) and cold-water temperatures (15, 20, 25, 30 and 35 °C). Each experiment was performed for 30 min after approaching steady state conditions. The outlet temperatures of feed and cold-water, module surface temperature, permeate temperature and permeate flow rate were measured.

Transmembrane flux can be defined as collected distillate volume as function of experimentation time ($\dot{V}_d$) and active area (A_m) of the membrane and can be determined with Eq. (3).

$$Flux = \frac{\dot{V}_d}{A_m} \quad (3)$$

Enthalpy changes of the feed (Q_f) and cold-water (Q_c) streams as shown in Eqs. (4) and (5) were used to determine thermal performance:

$$Q_f = \dot{m}_f c_p (T_{f,in} - T_{f,out}) \quad (4)$$

$$Q_c = \dot{m}_c c_p (T_{c,out} - T_{c,in}) \quad (5)$$

where $\dot{m}_f$ and $\dot{m}_c$ are the mass flow rates of feed and cold-water streams, respectively; $T_{f,in}$ and $T_{f,out}$ are feed inlet and outlet temperatures while cold-water inlet and outlet temperatures are denoted by $T_{c,in}$ and $T_{c,out}$. The heat capacity of water is termed as c_p (4180 J/kg K). For the calculations, it was assumed that the permeate contribution could be neglected, i.e. $\dot{m}_f \gg \dot{m}_d$ and $\dot{m}_c \gg \dot{m}_d$, where $\dot{m}_d$ is the permeate mass flow rate.

The specific thermal energy required ($\dot{Q}_f$)to operate MD system was determined in terms of heat demand per unit volume of the permeate ($\dot{V}_d$). The specific heat demand can be calculated using Eq. (6).

$$\dot{Q}_f = \frac{\dot{m}_f c_p (T_{f,in} - T_{f,out})}{\dot{V}_d} \quad (6)$$

Additionally, rate of heat transfer flow to the cold-water and heat transfer flow via convection and via permeate release were also determined using Eqs. (7)–(9).

Rate of heat transfer flow to cold-water ($\dot{Q}_c$) was calculated using Eq. (7).

$$\dot{Q}_c = \frac{\dot{m}_c c_p (T_{c,out} - T_{c,in})}{\dot{V}_d} \quad (7)$$

Moreover, rate of heat transfer flow from the module surface to the surrounding can be determined in terms of free convective heat transfer rate ($\dot{Q}_{cv}$) that was calculated using Eq. (8).

$$\dot{Q}_{cv} = \frac{hA(T_s - T_\infty)}{\dot{V}_d} \quad (8)$$

where h defines the heat transfer coefficient for free convection (approximately 10 W/m^2 K for natural convective cooling by air) and A is the area of the module surface.T_s defines the temperature at the surface of the module and T_∞ represents the atmospheric temperature at infinity point while taking module as the reference point.

The heat transfer rate of the distillate ($\dot{Q}_d$) was calculated with Eq. (9).

$$\dot{Q}_d = \frac{\dot{m}_d c_p (T_d - T_\infty)}{\dot{V}_d} \quad (9)$$

where T_d is defined as measured temperature of distillate.

2.2.3. Exergy analysis

Apart from energetic analysis, exergy analysis has also been performed in order to measure the extent of ideality and reversibility of the process. Considering the basic exergy definition, the exergy of each stream in the system can be calculated using following relations in Eqs. (10)–(14). Since the key parameters which effect the performance of the MD system are mainly temperatures and composition, therefore the kinetic and potential exergies were not determined.

$$Ex_{j,mechanical} = \dot{m}_j \frac{(P - P_R)}{\rho} \quad (10)$$

$$Ex_{j,thermal} = \dot{m}_j c_p \left[(T - T_R) - T_R \ln \frac{T}{T_R} \right] \quad (11)$$

$$Ex_{j,chemical} = -\dot{m}_j n_{solv} RT \ln \frac{n_{solv}}{\left(n_{solv} + \sum \frac{\beta_i C_i}{\rho m_{w,i}} \right)} \quad (12)$$

$$Ex_j = \dot{m}_j \left[\frac{P - P_R}{\rho} + c_p(T - T_R) - c_p T_R \ln \frac{T}{T_R} - n_{solv} RT \ln \frac{n_{solv}}{\left(n_{solv} + \sum \frac{\beta_i C_i}{\rho m_{w,i}} \right)} \right] \quad (13)$$

$$n_{solv} = \frac{\left[1000 - \sum \frac{C_i}{\rho} \right]}{m_{w,solv}} \quad (14)$$

In the above expressions, Ex_j represents total exergy of each stream , $\dot{m}_j$ shows the mass flow rate of each stream involved in the process, T_R and P_R depict the reference temperature and pressure respectively, P is total pressure and C_i defines the concentration of each contaminant/ solute. Moreover, $m_{w,i}$ and $m_{w,solv}$ show the molecular weight of each contaminant and solvent whereas n_{solv} presents the solvent concentration.

Exergies associated with the component's inlet and outlet streams are referred as inlet and outlet exergies of the specific component, respectively. Moreover, exergy change across any component of the MD system can be calculated from the differences in inlet streams exergies ($\sum Ex_{comp,in}$) and outlet streams exergies ($\sum Ex_{comp,out}$) and shown as irreversible exergy of that component ($Ex_{comp,ir}$) in Eq. (15).

$$Ex_{comp,ir} = \sum Ex_{comp,in} - \sum Ex_{comp,out} \quad (15)$$

Furthermore, ratio of minimum exergy required to the total actual exergy input provides the exergy efficiency of the MD system (η) which can be calculated using Eq. (16).

$$\eta = \frac{Ex_{f,in} - Ex_{f,out} - Ex_d}{Ex_{sys,in}} \times 100 \quad (16)$$

Additionally, irreversible exergies for each component and for the whole process were used to determine the contribution of each component of AGMD purification process towards total system irreversibility, mentioned as exergy destruction of the component ($Ex_{comp,des}$) in Eq. (17).

$$Ex_{comp,des} = \frac{Ex_{comp,ir}}{Ex_{sys,ir}} \times 100 \quad (17)$$

3. Results and discussion

The Xzero AGMD module performance was assessed mainly on the basis of the separation efficiency of the contaminants and permeate water quality. Transmembrane flux, thermal energy demand, energy distribution and exergy efficiency of the system are also presented in this section.

3.1. Separation efficiency

Table 2 presents the concentration of MD feed samples and the resulting permeate samples after 3 h of operation. The analysis results show that in all the MD feed samples ammonium ions (NH_4^+), potassium ions (K^+) and phosphate ions (PO_4^{-3}) were in high concentration, while except S1, the other two samples also have higher concentration of sulfate ions (SO_4^{-2}). The reason is addition of 10 mL of 40% sulfuric acid as neutralization solvent in the pre-treatment process for S2 and S3. In CMP wastewaters, the key contaminants were silicon (Si), aluminum (Al) and copper (Cu) as expected. Other than these contaminants, phosphorus (P) was also in high concentration.

The MD permeate analysis from all the three runs with different composition of CMP wastewaters shows the metal concentrations under detection limit except calcium (Ca), which was also reasonably low. The reduction of ammonium ions concentration in the permeate from S1 was not substantial (only ~25%) due to the presence of highly volatile ammonia vapor in S1. However, the addition of sulfuric acid in feed samples (S2 and S3) played an important role in reducing the volatility of ammonia gas, resulting in < 0.05 ppm of ammonium ions in permeate. Thus, the pretreatment of feed samples shows three times better rejection performance in case of ammonium ions. For other contaminants, the outcomes show non-detectable concentration of sodium ions, potassium ions, nitrate ions, chloride ions and fluoride ions in the permeate along with very low levels of phosphate (0.03 ppm in S1). Moreover, in case of sulfate ions, the MD shows remarkable results in terms of separation efficiency i.e., < 0.1 ppm.

Since the permeate was released from the MD system, the volume reduction of the initial feed samples led to an increase in retenate concentration. The concentration levels of the contaminants in MD retentate samples are summarized in Fig. 3. The outcomes are for three tests of S1, S2 and S3, which were run for 3 h. The concentrations of ions and metals were increased in the initial feed over time, as expected. However, chloride ions and nickel shows a slightly different trend of concentration change compared to other contaminants. For both of them, the initial feed shows higher concentration as compared to the concentrated retentate. The probability could be that these contaminants might be adsorbed on the membrane surface. (Follow-on studies would be needed to study this effect in more detail.)

It is clear from the outcomes presented in Table 3 that the D1 has high pH (~8) which corresponds to the presence of both NH_3 vapor (~10%) and NH_4^+ ions (~90%) in the permeate [55,56]. Moreover, the conductivity reduction was only 37%, and TC and COD removal were 77% and 62%, respectively. While comparing the pre-neutralized CMP wastewater S2 with the resulting permeate D2, it is found that the reduction in CMP wastewater pH (~3) has clearly an impact on the reversible reaction of ammonia-water (Eq. (15)) which means the expected equilibrium shift of NH_3 towards NH_4^+ ions might observed.

$$NH_4^+ + OH^- \rightleftarrows NH_3 + H_2O \quad (15)$$

Since volatility of the NH_3 is highly dependent on pH, therefore the better MD performance was obtained (permeate pH ~ 5.4 and conductivity 2.1 μS/cm). Furthermore, the TOC, TDS and COD were reduced up to 96%, 99.8% and 97.8% respectively. Considering sample S3, which was introduced in MD set up at relatively low temperature (75 °C), permeate (D3) water quality is also quite satisfactory. For instance, the conductivity was decreased up to 98.8% and TC reduction was reached to 82%. Moreover, TDS and COD were reduced $> 99.9\%$.

When comparing overall separation efficiency performance, MD shows very encouraging results for CMP wastewater treatment as compared to other available methods. Table 4 shows the comparison of MD with potential technologies including electro micro-filtration [19] and combination of electro-dialysis and RO [20]. For other related membrane based technologies i.e., integration of UF and RO was found to have comparable performance i.e., the reported conductivity was 5–6 μS/cm and TOC was 1.2–1.6 ppm [28].

3.2. Transmembrane flux

Fig. 4 shows the effect of varying feed flow rates and cold-water flow rates on transmembrane flux. In these experiments, the feed and cold-water temperatures were considered constant i.e., 80 °C and 25 °C, respectively. However, the feed flow rates ranged between 3.5 L/min to 7.2 L/min while the cold-water flow rate was held constant at 8.3 L/min in the first set of experiments. In the second set, the cold-water flow rates were varied from 3.5 to 8.3 L/min while considering the constant feed flow rate of 7.2 L/min. The reported transmembrane fluxes were measured when MD system approached steady state i.e., approximately after 60 minutes of operation.

The results obtained from first set of experiments show that with increasing feed flow rate, the transmembrane flux increases and

Table 2
Concentration of ionic and metallic contaminants in MD feed water samples and distillate samples (elapsed time of 3 h) in three tests. D represents distillate/permeate.

	Test 1		Test 2		Test 3	
Contaminants	S1	D1	S2	D2	S3	D3
Ions						
Sodium (ppm)	1.093	< 0.05	1.9	< 0.05	2.12	< 0.05
Ammonium (ppm)	16.6	12.4	26.57	< 0.05	30.2	< 0.05
Potassium (ppm)	8.5	< 0.05	14.2	< 0.05	19.9	< 0.05
Fluoride (ppm)	< 0.05	< 0.05	< 0.05	< 0.05	0.087	< 0.05
Chloride (ppm)	1.3	< 0.05	1.1	< 0.05	5.9	< 0.05
Nitrate (ppm)	0.84	< 0.1	0.18	< 0.1	0.5	< 0.1
Sulphate (ppm)	1.9	< 0.1	115.3	< 0.1	266.8	< 0.1
Phosphate (ppm)	12.26	0.037	9.7	< 0.01	32.07	< 0.01
Metals						
Aluminum (ppm)	9.9	< 0.0004	0.64	< 0.0004	1.23	< 0.0004
Calcium (ppm)	0.254	0.001	0.36	0.005	0.25	0.006
Potassium (ppm)	10.82	< 0.01	10.69	< 0.01	15.9	< 0.01
Chromium (ppm)	0.004	< 0.002	< 0.002	< 0.002	< 0.002	< 0.002
Manganese (ppm)	< 0.001	< 0.001	0.002	< 0.001	< 0.001	< 0.001
Iron (ppm)	0.025	< 0.001	0.39	< 0.001	0.02	< 0.001
Nickel (ppm)	0.057	< 0.005	0.034	< 0.005	0.017	< 0.005
Cobalt (ppm)	< 0.002	< 0.002	0.028	< 0.002	< 0.002	< 0.002
Copper (ppm)	3.5	< 0.004	4.9	< 0.004	3.05	< 0.004
Zinc (ppm)	0.054	< 0.002	0.048	< 0.002	0.006	< 0.002
Gallium (ppm)	< 0.015	< 0.015	0.09	< 0.015	< 0.015	< 0.015
Strontium (ppm)	0.001	< 0.0005	< 0.0005	< 0.0005	< 0.0005	< 0.0005
Phosphorous (ppm)	3.9	< 0.04	2.73	< 0.04	9.04	< 0.04
Germanium (ppm)	0.06	< 0.01	0.014	< 0.01	< 0.01	< 0.01
Tungsten (ppm)	0.022	< 0.01	< 0.01	< 0.01	< 0.01	< 0.01
Titanium (ppm)	< 0.04	< 0.04	< 0.04	< 0.04	< 0.04	< 0.04
Silicon (ppm)	95.16	< 0.1	6.4	< 0.1	0.27	< 0.1
Tantalum (ppm)	0.271	< 0.01	< 0.01	< 0.01	0.062	< 0.01
Zirconium (ppm)	< 0.005	< 0.005	< 0.005	< 0.005	< 0.005	< 0.005

‘ < ’ indicates a value below the respective detection limit.

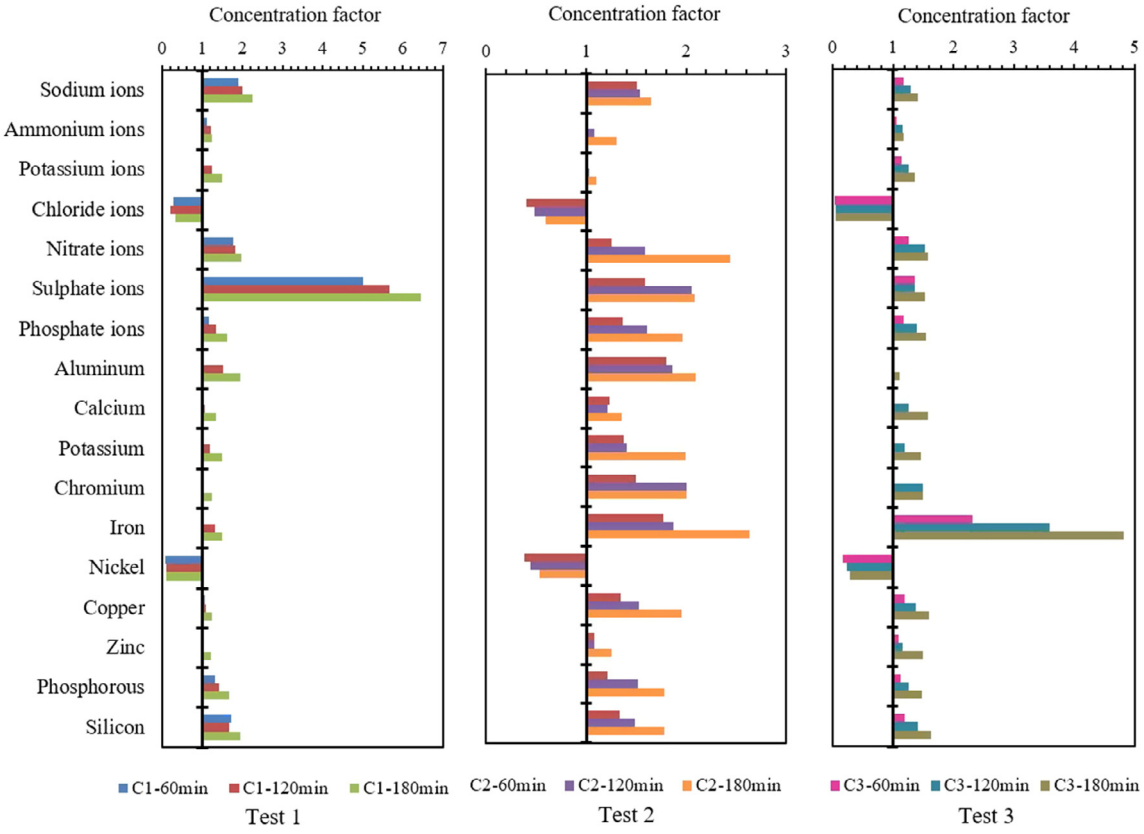

Fig. 3. Concentration levels of the three MD feed water samples and corresponding concentrated streams after each hour during 3 h elapsed time. C represents concentrate/retentate.

Table 3
Water quality parameters for the three MD feed water samples and corresponding distilled water and concentrated streams (elapsed time of 3 h). C and D represent concentrate/retentate and distillate/permeate, respectively.

	Test 1			Test 2			Test 3		
	S1	C1	D1	S2	C2	D2	S3	C3	D3
VRF	0.32			0.33			0.3		
Conductivity (μS/cm)	120	186.4	75.6	774	1020	2.1	1580	1972	18.5
pH	6.6	7.6	8	3	2.9	5.4	2.6	2.4	4.4
TOC (ppm)	31.4	33	1.06	30.3	35.6	1.1	24.3	27.6	4.9
IC (ppm)	9.5	9.9	8.3	0.3	0.252	0.2	0.2	0.2	0.2
TC (ppm)	40.9	42.9	9.36	30.6	35.85	1.3	24.5	27.8	5.1
TDS (ppm)	86.4	147.2	32.5	534.06	826.2	1.1	1036.4	1482.9	7.2
COD (ppm)	94.2	220	1.8	90.9	237.3	1.9	82.8	162	8.5

Table 4
Comparison of performance of different technologies for CMP wastewater treatment.

Technologies	Electro-microfiltration	Electro- dialysis and Reverse osmosis	Neutralization and Membrane Distillation
References	[19]	[20]	Present Study
Si (ppm)	79.81	2	< 0.1
Al (ppm)	0.09	0.06–0.13	< 0.0004
Fe (ppm)	0.12	0.13–0.21	< 0.001
Cu (ppm)	0.19	0.05–0.15	< 0.004
Ca (ppm)	0.03	0.03–0.1	0.005
K (ppm)	21.3	5	< 0.01
pH	9.84	4.8–10.8	4.4–5.4
Conductivity (μS/cm)	145.1	43	2.1–18.5
TOC (ppm)	1.65	1.8–2.9	1.1–4.9
TDS (ppm)	62.2	22	1.1–7.2

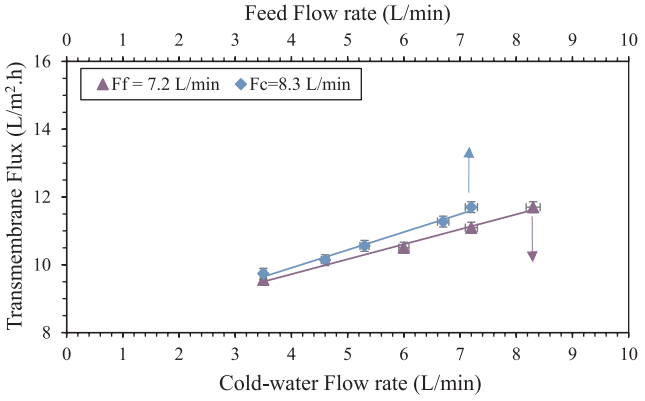

Fig. 4. Variation of transmembrane flux as a function of MD feed and cold-water flow rates while considering the other one constant. (Constant feed flow rate (Ff) was 7.2 L/min and constant cold-water (Fc) flow rate was 8.3 L/min). MD feed temperature was 80°C and cold-water temperature was 25 °C.

presents the positive linear trend because the higher bulk temperature is maintained along the feed flow path and due to decrease in the boundary layer resistance. The increase in the transmembrane flux was observed from 9.7 to 11.7 L/m^{2}h while almost doubling the feed flow rate (from 3.5 L/min to 7.2 L/min) in line with the results published by Baaklini [57].

Moreover, it was observed from the second set of experiments that the reduction in cold-water flow rate provides the lower transmembrane flux at the constant feed flow rates. The lower cold-water flow rate indicates the lower heat recovering capacity from the distillate water vapors. This leads to lower extent of condensation happing in the air gap of the MD system.

Fig. 5 demonstrates the effect of the feed temperature on

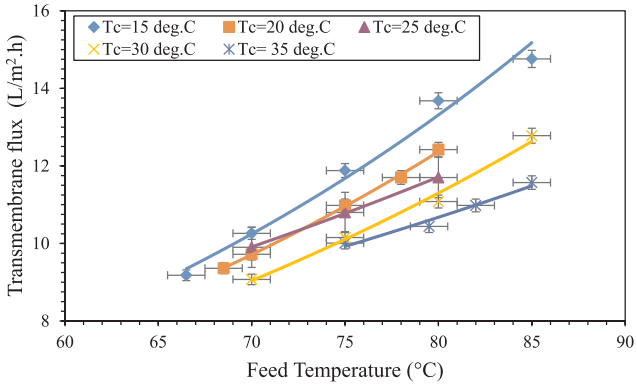

Fig. 5. Effect of MD feed and cold-water temperatures on transmembrane flux considering constant MD feed flow rate of 7.2 L/min and constant cold-water flow rate of 8.3 L/min.

transmembrane flux while considering constant feed and cold-water flow rates (7.2 L/min and 8.3 L/min, respectively) and varying cold-water temperature (15–40 °C). The outcomes indicate that the transmembrane flux adopts linear to weakly exponential increasing trend with increasing feed inlet temperature. The observed trends can be linked to lower viscosity of water at higher temperatures along with changes in the relationship between the vapor pressure and feed temperature, as defined by the Antoine equation illustrated in Eq. (16).

$$\ln p_v = A + \frac{B}{C + T_f} \quad (16)$$

where A, B and C are the regression constants for the specific compounds, p_v and T_f represent vapor pressure and temperature of feed, respectively. For water, A = 23.238; B = 3841; C = 45.

The same feed to cold-water temperature difference (defined by different feed and cold-water temperatures) results in different values of vapor pressure difference which effects directly on the transmembrane flux. The transmembrane flux was maximum at feed temperature of 85 °C and cold-water temperature of 15 °C. These temperatures provide the highest extent of driving force as compared to other scenarios.

Since CMP wastewater samples were quite diluted, therefore, fouling phenomenon was not observed as expected during the elapsed time. However, follow-on studies would be needed to investigate this phenomenon in more detail.

3.3. Energy analysis

An energy analysis of the AGMD unit was performed by considering the specific thermal energy demand as the key parameter. Fig. 6 presents specific thermal energy demand values for varying feed and cold-water inlet temperatures while considering constant feed and cold-water flow rates i.e., 7.2 L/min and 8.3 L/min, respectively. Specific

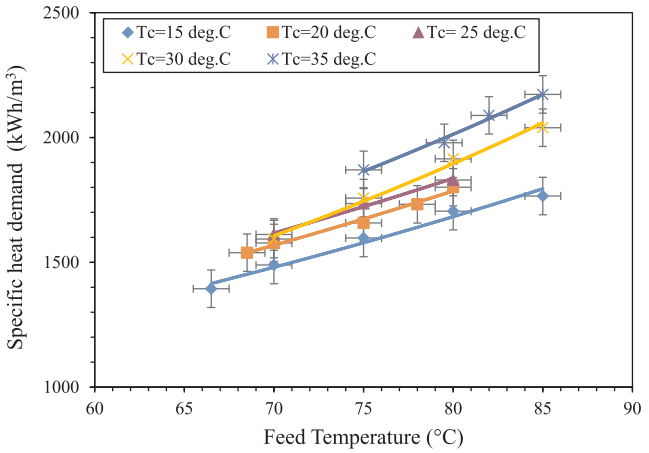

Fig. 6. Effect of MD feed and cold-water temperatures on specific heat demand considering constant MD feed flow rate of 7.2 L/min and constant cold-water flow rate of 8.3 L/min.

heat demand values show a positive linear trend while increasing feed temperature and keeping cold-water temperature constant. The fact behind is higher heat transfer rate from the feed to permeate region across the membrane which results in higher temperature difference between feed inlet and outlet streams ($T_{f,in}$ - $T_{f,out}$) at elevated feed temperatures. While comparing different cold-water temperatures at constant feed temperature, a similar trend can be observed i.e., an increase in cold-water temperatures results in higher specific thermal energy demand. The reason is the lower transmembrane flux across the membrane at higher cold-water temperature associated with lower feed to coolant temperature difference. Thus, specific heat demand significantly increases with higher feed inlet temperature and higher cold-water inlet temperature i.e., 1390–2170 kWh/m^3 in agreement with the values presented by Baaklini [57] and Woldemariam & Martin [54]. In the present and referred studies, relatively higher specific heat demand was observed due to absence of heat recovery systems in laboratory based units [58]. The specific heat demand can be reduced in large-scale equipment when internal heat recovery concept is introduced while adding stages in series [46,59], using thermal storage to recover surplus energy or considering concentrate recycle loop [60].

Furthermore, specific heat transfer flow rates to cold-water and via permeate and convection were also determined and presented in Table 5 for constant feed inlet temperature of 80 °C and varying cold-water temperature between 15 °C and 35 °C. The calculations show that approximately 90% of the total specific thermal energy was transferred indirectly to the cold-water circulating through the cooling plates. The rest of the total specific thermal energy was accounted for energy stored in the distillate, lost due to convection and lost through the pipe walls, valves and joints.

Although higher driving force at lower cold-water temperatures (i.e., 15 °C) was associated with higher transmembrane flux, however, the permeate temperature was lower as compared to when the cold-water temperature was higher i.e., 35 °C. Therefore, with increasing cold-water temperature, specific heat transfer flow rate via permeate release is relatively higher. Moreover, the similar trend can be observed for convective heat transfer that indicates higher specific heat transfer flow rate from the module surfaces at elevated cold-water temperatures. The specific heat transfer flow rate to the cold-water also increases at higher cold-water temperature due to lower transmembrane flux.

Table 5
Effect of cold-water temperature on specific heat transfer flow rates to cold-water and via permeate and convection at constant feed inlet temperature of 80 °C.

Cold-water temperature (°C)	$\dot{Q}_c$ (kWh/m^3)	$\dot{Q}_{cv}$ (kWh/m^3)	$\dot{Q}_d$ (kWh/m^3)
15	1574	38	19
20	1660	45	20
25	1683	52	22
30	1763	58	25
35	1813	66	27

Table 6
Exergy flow rates of each component of Xzero air gap membrane distillation bench scale unit.

Main Components	$Ex_{comp,in}$ (kW)	$Ex_{comp,out}$ (kW)
Recirculation tank	3.68	2.44
Hot water pump	2.45	2.44
Membrane distillation module	2.49	1.42
Cold-water pump	0.047	0.046
Cold-water tank	1.87	0.047

3.4. Exergy efficiency

Along with energy analysis, exergy efficiency was also determined in this study. The considered operating conditions include MD feed inlet flow rate of 7.2 L/min, cold-water inlet flow rate of 8.3 L/min, MD feed inlet temperature of 80 °C and cold-water inlet temperature of 30 °C. Moreover, the chemical composition and concentration of sample S2 has been considered for calculating total exergy flow rates. The total exergy flow rates are shown in Table 6 for each component.

Furthermore, it was found that the exergy efficiency of the whole unit was 19%, which is comparable to the published results [61]. Each component in the unit is typically accountable for certain percentage of the total irreversibility produced. The results show that recirculation tank is responsible for ~ 32% of total exergy destruction. Heat losses through the recirculation tank walls and evaporation through the tank cover openings are responsible for the exergy destruction in the hot recirculation tank. The cold-water tank share was ~ 48% of total exergy destruction, which was comparatively higher since the cold-water tank was uncovered. MD module was accountable of ~ 20% exergy destruction due to heat losses through condensation walls and the heat transfer through conduction, convection and permeate release. These results indicate the need of optimized MD unit in terms of its membrane material, insulation and condensation plates design. Moreover, the performance of recirculation tank and cooling water tank can be improved using proper insulation in order to reduce evaporative and conductive losses.

4. Concluding remarks

The study presents the potential of membrane distillation (MD) technology for treatment of chemical mechanical planarization wastewater from nano-electronics industries. Case study of imec, Belgium has been selected for the purpose and Xzero MD prototype was used for experimental studies. Considering the performance of MD unit in terms of treated water quality, different parameters have been reported including the compositional analysis, concentration, conductivity, pH, TOC, TDS and COD however, in terms of technical assessment of the methods transmembrane flux, specific heat demand, energy distribution and exergy efficiency were determined while varying different operating parameters (feed and cold-water flow rates and temperatures). The outcomes depict that high quality permeate was recovered having major contaminants (silicon, aluminum and copper) concentration below the detection limit, conductivity ~2.11 μS/cm, pH ~ 5.4, TOC ~ 1.13 ppm, IC ~ 0.24 ppm, TDS ~ 1.1 ppm and COD ppm ~ 1.9 while considering neutralization prior to membrane distillation at MD feed flow rate of 7.2 L/min and temperature of 80°C and cold-water flow rate of 8.3 L/min and temperature of 30 °C. From the

parametric analysis, the maximum flux achieved was 14.8 L/m^{2}h at the feed to cold-water temperature difference of 70 °C. The specific heat demand was varied between 1390 and 2170 kWh/m^3 depending on the feed temperature and feed to cold-water temperature difference. Moreover, the estimated exergy efficiency of Xzero AGMD prototype was ~19%.

Acknowledgements

This research has been conducted in collaboration between KTH Royal Institute of Technology, Sweden and Aalto University, Finland, funded through Erasmus Mundus Joint Doctorate Programme "Environomical Pathways for Sustainable Energy Services", under the Framework Partnership Agreement FPA-2012-0034 between Education, Audiovisual and Culture Executive Agency (EACEA) and KTH as Coordinating Partner of the SELECT + Consortium. The case study has also been supported by the industrial partners including Xzero AB, Sweden and Interuniversity Microelectronics Center (imec), Belgium. This publication reflects the views only of the author(s) and mentioned organizations cannot be held responsible for any use, which may be made of the information contained therein.

Declaration of Competing Interest

The authors declare no conflict of interest.

References

[1] K.D. Beyer, "A" dirty" risk, Innov. Lead. 8 (1999) 407.
[2] D.E. Speed, Environmental Aspects of Planarization ProcessesAdvances in Chemical Mechanical Planarization (CMP), Woodhead Publishing, 2016, pp. 229–269.
[3] W.G. America, S.V. Babu, Slurry additive effects on the suppression of silicon nitride removal during CMP, Electrochem. Solid-State Lett. 7 (12) (2004) 327–330.
[4] M. Krishnan, J.W. Nalaskowski, L.M. Cook, Chemical mechanical planarization: slurry chemistry, materials, and mechanisms, Chem. Rev. 110 (1) (2010) 178–204.
[5] T. Du, Y. Luo, V. Desai, The combinatorial effect of complexing agent and inhibitor on chemical-mechanical planarization of copper, Microelectron. Eng. 71 (1) (2004) 90–97.
[6] G.B. Basim, Effect of slurry aging on stability and performance of chemical mechanical planarization process, Adv. Powder Technol. 22 (2) (2011) 257–265.
[7] S. Armini, C.M. Whelan, M. Moinpour, K. Maex, Mixed organic/inorganic abrasive particles during oxide CMP, Electrochem. Solid-State Lett. 11 (7) (2008) 197–201.
[8] D.E. Speed, Environmental Aspects of Planarization Processes, Advances in Chemical Mechanical Planarization (CMP), Woodhead Publishing, 2016, pp. 229–269.
[9] J.-C. Tsai, M. Kumar, S.-Y. Chen, J.-G. Lin, Nano-bubble flotation technology with coagulation process for the cost-effective treatment of chemical mechanical polishing wastewater, Sep. Purif. Technol. 58 (1) (2007) 61–67.
[10] W. Den, C. Huang, Electrocoagulation for removal of silica nano-particles from chemical–mechanical-planarization wastewater, Colloids Surf. A Physicochem. Eng. Asp. 254 (1–3) (2005) 81–89.
[11] R. Lo, S.-L. Lo, A pilot plant study using ceramic membrane microfiltration, carbon adsorption and reverse osmosis to treat CMP (chemical mechanical polishing) wastewater, Water Sci. Technol. Water Supply 4 (1) (2004) 111–118.
[12] C.L. Lai, S.H. Lin, Treatment of chemical mechanical polishing wastewater by electrocoagulation: system performances and sludge settling characteristics, Chemosphere 54 (3) (2004) 235–242.
[13] G. Corlett, Targeting water use for chemical mechanical polishing, Solid State Technol 43 (6) (2000) 201–202.
[14] Council Directive 91/271/EEC, Urban waste water treatment. 1991.
[15] G.C.C. Yang, CMP watewater management using the concepts of design for environment, Environ. Prog. 21 (1) (2002) 57–62.
[16] X. Wu, X. Ge, D. Wang, H. Tang, Distinct coagulation mechanism and model between alum and high Al13-PACl, Colloids Surf. A Physicochem. Eng. Asp. 305 (1–3) (2007) 89–96.
[17] B.M. Belongia, P.D. Haworth, J.C. Baygents, S. Raghavan, Treatment of alumina and silica chemical mechanical polishing waste by electrodecantation and electrocoagulation, J. Electrochem. Soc. 146 (11) (1999) 4124–4130.
[18] C.L. Lai, S.H. Lin, Electrocoagulation of chemical mechanical polishing (CMP) wastewater from semiconductor fabrication, Chem. Eng. J. 95 (1) (2003) 205–211.
[19] G.C. Yang, T.-Y. Yang, S.-H. Tsai, Crossflow electro-microfiltration of oxide-CMP wastewater, Water Res. 37 (4) (2003) 785–792.
[20] G.C. Yang, T.-Y. Yang, Reclamation of high quality water from treating CMP wastewater by a novel crossflow electrofiltration/electrodialysis process, J. Memb. Sci. 233 (1–2) (2004) 151–159.
[21] C.Y. Hu, S.L. Lo, C.M. Li, W.H. Kuan, Treating chemical mechanical polishing (CMP) wastewater by electro-coagulation-flotation process with surfactant, J. Hazard. Mater. 120 (1–3) (2005) 15–20.
[22] W. Den, C. Huang, Electrocoagulation for removal of silica nano-particles from chemical–mechanical-planarization wastewater, Colloids Surf. A Physicochem. Eng. Asp. 254 (1–3) (2005) 81–89.
[23] Y.-H. Liu, C.-Y. Lin, J.-H. Huang, S.-C. Yen, Particle removal performance and its kinetic behavior during oxide-CMP wastewater treatment by electrocoagulation, J. Taiwan Inst. Chem. Eng. 60 (2016) 520–524.
[24] C.-T. Wang, W.-L. Chou, L.-S. Chen, S.-Y. Chang, Silica particles settling characteristics and removal performances of oxide chemical mechanical polishing wastewater treated by electrocoagulation technology, J. Hazard. Mater. 161 (1) (2009) 344–350.
[25] W.-L. Chou, C.-T. Wang, W.-C. Chang, S.-Y. Chang, Adsorption treatment of oxide chemical mechanical polishing wastewater from a semiconductor manufacturing plant by electrocoagulation, J. Hazard. Mater. 180 (1) (2010) 217–224.
[26] E.L.S.S. Browne, V. Krygier, J. O'Sullivan, Treating wastewater from CMP using ultrafiltration, MICRO (1999) 78–86.
[27] S.H. Lin, C.R. Yang, Chemical and physical treatments of chemical mechanical polishing wastewater from semiconductor fabrication, J. Hazard. Mater. 108 (1) (2004) 103–109.
[28] L.-C. Juang, D.-H. Tseng, H.-Y. Lin, C.-K. Lee, T.-M. Liang, Treatment of chemical mechanical polishing wastewater for water reuse by ultrafiltration and reverse osmosis separation, Environ. Eng. Sci. 25 (7) (2008) 1091–1098.
[29] T.-J. Wan, S.-M. Shen, S.-H. Siao, C.-F. Huang, C.-Y. Cheng, Using magnetic seeds to improve the aggregation and precipitation of nanoparticles from backside grinding wastewater, Water Res. 45 (19) (2011) 6301–6307.
[30] Y.G. Kim, J.B. Song, D.G. Yang, W.J. Kim, S.H. Kim, H. Lee, Purification of chemical mechanical polishing wastewater via superconducting high gradient magnetic separation system with optimal coagulation process, IEEE Trans. Appl. Supercond. 25 (3) (2015) 1–5.
[31] K.W. Lawson, D.R. Lloyd, Membrane distillation, J. Memb. Sci. 124 (1) (1997) 1–25.
[32] A. Alkhudhiri, N. Darwish, N. Hilal, Membrane distillation: a comprehensive review, Desalination 287 (2012) 2–18.
[33] A.M. Alklaibi, N. Lior, Membrane-distillation desalination: status and potential, Desalination 171 (2) (2005) 111–131.
[34] M. Khayet, T. Matsuura, Membrane Distillation: Principles and Applications, Elsevier, 2011.
[35] P. Onsekizoglu, Membrane distillation: Principle, advances, limitations and future prospects in food industry, Distill, Adv. from Model. to Appl. (2012) 233–266.
[36] B. Jiao, A. Cassano, E. Drioli, Recent advances on membrane processes for the concentration of fruit juices: a review, J. Food Eng. 63 (3) (2004) 303–324.
[37] H.C. Duong, et al., A novel application of membrane distillation to facilitate nickel recovery from electroplating wastewater, Environ. Sci. Pollut. Res. 26 (23) (2019) 23407–23415.
[38] H. Attia, S. Alexander, C.J. Wright, N. Hilal, Superhydrophobic electrospun membrane for heavy metals removal by air gap membrane distillation (AGMD), Desalination 420 (2017) 318–329.
[39] I-. Noor, J. Coenen, A. Martin, O. Dahl, M. Åslin, Experimental investigation and techno-economic analysis of tetramethylammonium hydroxide removal from wastewater in nano-electronics manufacturing via membrane distillation, J. Memb. Sci., Jun. 579 (2019) 283–293.
[40] Y. Wu, Y. Kang, L. Zhang, D. Qu, X. Cheng, L. Feng, Performance and fouling mechanism of direct contact membrane distillation (DCMD) treating fermentation wastewater with high organic concentrations, J. Environ. Sci. 65 (2018) 253–261.
[41] T.L.S. Silva, et al., Desalination and removal of organic micropollutants and microorganisms by membrane distillation, Desalination 437 (2018) 121–132.
[42] Y. Nleya, G.S. Simate, S. Ndlovu, Sustainability assessment of the recovery and utilisation of acid from acid mine drainage, J. Clean. Prod. 113 (2016) 17–27.
[43] X. Feng, L.Y. Jiang, Y. Song, Titanium white sulfuric acid concentration by direct contact membrane distillation, Chem. Eng. J. 285 (2016) 101–111.
[44] U.K. Kesieme, H. Aral, Application of membrane distillation and solvent extraction for water and acid recovery from acidic mining waste and process solutions, J. Environ. Chem. Eng. 3 (3) (2015) 2050–2056.
[45] K. Gethard, O. Sae-Khow, S. Mitra, Carbon nanotube enhanced membrane distillation for simultaneous generation of pure water and concentrating pharmaceutical waste, Sep. Purif. Technol. 90 (2012) 239–245.
[46] D. Woldemariam, A. Kullab, U. Fortkamp, J. Magner, H. Royen, A. Martin, Membrane distillation pilot plant trials with pharmaceutical residues and energy demand analysis, Chem. Eng. J. 306 (2016) 471–483.
[47] J. Kim, J. Kim, S. Hong, Recovery of water and minerals from shale gas produced water by membrane distillation crystallization, Water Res. 129 (2018) 447–459.
[48] M. Laqbaqbi, M.C. García-Payo, M. Khayet, J. El Kharraz, M. Chaouch, Application of direct contact membrane distillation for textile wastewater treatment and fouling study, Sep. Purif. Technol. 209 (2019) 815–825.
[49] Z. Yan, et al., Treatment of anaerobic digestion effluent using membrane distillation: Effects of feed acidification on pollutant removal, nutrient concentration and membrane fouling, Desalination 449 (2019) 6–15.
[50] F. Li, et al., Direct contact membrane distillation for the treatment of industrial dyeing wastewater and characteristic pollutants, Sep. Purif. Technol. 195 (2018) 83–91.
[51] A. Ali, C.A. Quist-Jensen, E. Drioli, F. Macedonio, Evaluation of integrated microfiltration and membrane distillation/crystallization processes for produced water treatment, Desalination 434 (2018) 161–168.
[52] B. Ozbey-Unal, D.Y. Imer, B. Keskinler, I. Koyuncu, Boron removal from geothermal water by air gap membrane distillation, Desalination 433 (2018) 141–150.
[53] H. Dolfe, Xzero AB. Personal Communication, 2018.

[54] D. Woldemariam, A. Kullab, E.U. Khan, A. Martin, Recovery of ethanol from scrubber-water by district heat-driven membrane distillation: Industrial-scale technoeconomic study, Renew. Energy 128 (2018) 484–494.
[55] A.G. Capodaglio, P. Hlavínek, M. Raboni, Physico-chemical technologies for nitrogen removal from wastewaters: a review, Revista Ambiente & Água ,10 (2015) 481–498.
[56] K. Emerson, R.C. Russo, R.E. Lund, R.V. Thurston, Aqueous ammonia equilibrium calculations: effect of pH and temperature, J. Fish. Board Canada 32 (12) (1975) 2379–2383.
[57] D. Baaklini, Performance analysis of Air GapMembrane Distillation: Comparison of PTFE membranes: Comparison of PTFE membranes, Master Thesis Report, KTH Royal Institute of Technology, 2011.
[58] M. Khayet, Solar desalination by membrane distillation: dispersion in energy consumption analysis and water production costs (a review), Desalination 308 (2013) 89–101.
[59] E. Guillén-Burrieza, et al., Experimental analysis of an air gap membrane distillation solar desalination pilot system, J. Memb. Sci. 379 (1–2) (2011) 386–396.
[60] R.B. Saffarini, E.K. Summers, H.A. Arafat, J.H. Lienhard V, Technical evaluation of stand-alone solar powered membrane distillation systems, Desalination, 286 (2012) pp. 332–341.
[61] D. Woldemariam, A. Martin, M. Santarelli, Exergy analysis of air-gap membrane distillation systems for water purification applications, Appl. Sci. 7 (3) (2017) 301.